A LINEAR PAM-BASED RECEIVER FOR MULTI-H CPM

Erik Perrins
Department of Electrical and Computer Engineering
Brigham Young University
Provo, UT 84602
esp@ee.byu.edu

Faculty Advisor:
Michael Rice

ABSTRACT

A linear pulse-amplitude modulation (PAM) receiver for the ARTM Tier II multi-h waveform is presented. The receiver is optimal and can be implemented using maximum likelihood sequence estimation (MLSE). The linear signal model also allows many attractive complexity reductions. The performance of these reduced-complexity receivers is evaluated via computer simulation. One simplified receiver consists of three matched filters and a 32-state Viterbi trellis and is shown to perform with a 1.5 dB degradation relative to the optimal receiver.

INTRODUCTION

The Advanced Range Telemetry (ARTM) Tier II modulation format is multi-h continuous phase modulation (CPM). Some of the attractive features of this modulation format are that it has constant envelope and narrow bandwidth [1]. However, the existing optimal MLSE receiver for CPM [2] can require a large number of matched filters and trellis states. This is due to the non-linear nature of the modulation. For the ARTM Tier II modulation, the optimal receiver requires a set of 64 matched filters for each modulation index, and a 512-state trellis.

In this paper, a new receiver for multi-h CPM is presented which is based on a PAM representation, and is an extension of previous work [3, 4] to the multi-h case. The receiver is optimal in the MLSE sense, but offers no complexity reduction as it requires a set of 48 matched filters for each modulation index and uses the same 512-state trellis as the existing MLSE receiver. However, the linear PAM signal model

allows for various complexity reduction techniques. One receiver presented reduces the number of states from 512 to 32, and the number of matched filters from two sets of 48 to a single set of three 3 filters, with a performance degradation of 1.5 dB at BER $= 10^{-5}$. Another strength of the linear decomposition is that it preserves the gain which multi-h CPM achieves over single-h CPM. This gain is lost in other complexity-reduction techniques [2, 5].

In the following, the CPM signal is described. The linear PAM decomposition is then summarized for the ARTM Tier II case. The optimal MLSE receiver is presented, along with the various complexity-reduction techniques. The performance of these receivers is evaluated with computer simulations. The results are summarized and conclusions are presented.

CPM SIGNAL MODEL

CPM refers to a general class of digitally modulated signals in which the phase is constrained to be continuous. The complex-baseband signal may be expressed as

$$s(t) = \exp\big(j\psi(t,\boldsymbol{\alpha})\big) \tag{1}$$

$$\psi(t,\boldsymbol{\alpha}) = 2\pi \sum_{i=-\infty}^{n} \alpha_i h_{(i)} q(t-iT), \qquad nT < t < (n+1)T \tag{2}$$

where T is the symbol duration, $h_{(i)}$ are the modulation indices, $\boldsymbol{\alpha} = \{\alpha_i\}$ are the information symbols in the M-ary alphabet $\{\pm 1, \pm 3, \cdots, \pm(M-1)\}$, and $q(t)$ is the phase pulse. The subscript notation on the modulation indices is defined as

$$h_{(i)} \equiv h_{(i \bmod N_h)} \tag{3}$$

where N_h is the number of modulation indices (for the special case of single-h CPM, $N_h = 1$). The phase pulse $q(t)$ is related to the frequency pulse $f(t)$ by the relationship

$$q(t) = \int_0^t f(\tau)\, d\tau. \tag{4}$$

The frequency pulse is time-limited to the interval $(0, LT)$ and is subject to the constraints

$$f(t) = f(LT - t), \qquad \int_0^{LT} f(\tau)\, d\tau = q(LT) = \frac{1}{2}. \tag{5}$$

In light of the constraints on $f(t)$ and $q(t)$, Equation (2) can be written as

$$\psi(t,\boldsymbol{\alpha}) = \theta(t,\boldsymbol{\alpha}_n) + \theta_{n-L} = 2\pi \sum_{i=n-L+1}^{n} \alpha_i h_{(i)} q(t-iT) + \pi \sum_{i=-\infty}^{n-L} \alpha_i h_{(i)} \bmod 2\pi. \tag{6}$$

The term $\theta(t,\boldsymbol{\alpha}_n)$ is a function of the L symbols being modulated by the phase pulse. For $h_{(i)} = 2k_{(i)}/p$ ($k_{(i)}$, p integers), the phase state θ_{n-L} takes on p distinct values $0, 2\pi/p, 2 \cdot 2\pi/p, \ldots, (p-1)2\pi/p$. The total number of states is pM^{L-1}, with M branches at each state. Each branch is defined by the $L+1$-tuple

$\sigma_n = (\theta_{n-L}, \alpha_{n-L+1}, \alpha_{n-L+2}, \ldots, \alpha_n)$. The ARTM Tier II modulation is $M = 4$, $h = \{4/16, 5/16\}$ ($N_h = 2$), 3RC (raised cosine frequency pulse of length $L = 3$).

EQUIVALENT PAM REPRESENTATION OF THE ARTM TIER-II WAVEFORM

Laurent [3] showed that a binary CPM signal (i.e. $M = 2$) could be decomposed into a linear combination of PAM waveforms. The M-ary PAM representation was derived by Mengali [4], where he showed that the M-ary signal could be obtained by first applying the binary Laurent decomposition $P = \log_2 M$ times and then multiplying the parallel binary systems together. To obtain the PAM representation of a multi-h signal, the binary and M-ary decompositions are extended to obtain the expression

$$s(t, \boldsymbol{\alpha}) = \sum_{k=0}^{N-1} \sum_{i=n-D_k+1}^{n} a_{k,\,i}\, g_{k,(i)}(t - iT), \qquad nT \le t < (n+1)T \tag{7}$$

where the signal is a sum of pulses $g_{k,(i)}(t)$ scaled by the pseudo-symbols $a_{k,\,i}$, and each pulse is non-zero for a duration of $D_k T$. This expression differs from the single-h case in that a modulo-N_h time-index is added to $g_{k,(i)}(t)$. The definitions of $a_{k,\,i}$ and $g_{k,(i)}(t)$ will be summarized in this section for the ARTM Tier II case, with a more detailed description of the general multi-h case to appear in a later paper.

The 4-ary signal is obtained from two binary Laurent decompositions, indexed by l ($0 \le l \le 1$). The set of pseudo-symbols for each of these binary subsystems is given by

$$b_{k,\,n}^{(l)} = \exp\left\{ j\pi \left[\sum_{m=-\infty}^{n} h_{(m)}^{(l)} \gamma_{m,\,l} - \sum_{i=0}^{L-1} h_{(n-i)}^{(l)} \gamma_{n-i,\,l} \beta_{k,\,i} \right] \right\} \tag{8}$$

where the important feature is that the two binary data streams are scaled by different modulation indices $h_{(n)}^{(l)} = 2^l h_{(n)}$. Equation (8) shows that the scaled binary data symbols $h_{(n)}^{(l)} \gamma_{n,\,l}$ are fed into a summing filter and into a bank of FIR filters (indexed by k). The output of the k-th FIR filter is subtracted from the output of the summing filter, forming the exponent of the non-linearity $\exp\{j\pi(\cdot)\}$. The bank of $Q = 2^{L-1}$ FIR filters have taps given by the radix-2 decomposition of the index k

$$k = \sum_{i=1}^{L-1} 2^{i-1} \beta_{k,\,i}, \qquad 0 \le k \le Q - 1, \tag{9}$$

where $\beta_{k,\,0}$ is always zero. Table 1 gives the mapping from 4-ary symbols to binary symbols, and the FIR filter coefficients for the $L = 3$, $M = 4$ case (ARTM Tier II).

The signal pulses $g_{k,(n)}$ in Equation (7) are also obtained from the two binary decompositions. The function $u(t)$ is defined as

$$u(t) = \begin{cases} \sin\big(2\pi h q(t)\big) / \sin(\pi h) & 0 \le t \le LT \\ u(2LT - t) & LT \le t \le 2LT \\ 0 & \text{elsewhere.} \end{cases} \tag{10}$$

Table 1: Decomposition parameters for the $L = 3$, $M = 4$ case

α_n	$\gamma_{n,1}$	$\gamma_{n,0}$
-3	-1	-1
-1	-1	1
1	1	-1
3	1	1

k	$\beta_{k,2}$	$\beta_{k,1}$	$\beta_{k,0}$
0	0	0	0
1	0	1	0
2	1	0	0
3	1	1	0

This function can be divided into $2L$ segments, each of which has a duration of T

$$u_j(t) = u(jT + t), \qquad 0 \le t \le T, \quad 0 \le j \le 2L - 1. \tag{11}$$

In the ARTM Tier II multi-h case, we have $u_{j,(i)}(t)$, where we account for each $h_{(i)}$.

The binary Laurent pulses are $c_{k,(n)}(t)$, where $0 \le k \le Q - 1$. For the ARTM Tier II case, the modulo index (n) has two values, i.e. $c_{k,\,0}(t)$ and $c_{k,\,1}(t)$. The $k = 0$ pulse for "even" symbol intervals is

$$c_{0,\,0}(t) = \begin{cases} u_{0,\,0}(t)u_{1,\,1}(t)u_{2,\,0}(t) & 0 \le t \le T \\ u_{1,\,0}(t-T)u_{2,\,1}(t-T)u_{3,\,1}(t-T) & T \le t \le 2T \\ u_{2,\,0}(t-2T)u_{3,\,0}(t-2T)u_{4,\,1}(t-2T) & 2T \le t \le 3T \\ u_{3,\,1}(t-3T)u_{4,\,0}(t-3T)u_{5,\,1}(t-3T) & 3T \le t \le 4T \\ 0 & \text{elsewhere} \end{cases} \tag{12}$$

$$\equiv \; [u_{0,\,0}u_{1,\,1}u_{2,\,0};\; u_{1,\,0}u_{2,\,1}u_{3,\,1};\; u_{2,\,0}u_{3,\,0}u_{4,\,1};\; u_{3,\,1}u_{4,\,0}u_{5,\,1}]. \tag{13}$$

The entire set of pulses for both even and odd symbol intervals is shown in Table 2 using the compact notation defined in Equations (12)–(13). We define $c^{(l)}_{k,(n)}$ as the set of pulses from the l-th binary subsystem.

With the pseudo-symbols and pulses specified for the binary case, the 4-ary pseudo-symbols $a_{k,\,i}$ and pulses $g_{k,(i)}(t)$ are given by Table 3. These give an exact representation of the multi-h CPM signal in Equation (7). We also use Table 3 to recognize important characteristics of the pseudo-symbols. For example, the $k = 7$ entry shows that $a_{7,\,n} = b^{(0)}_{1,\,n}b^{(1)}_{0,\,n}$. From Equation (8) and Table 1, we see that

$$b^{(1)}_{0,\,n} = \exp\left\{ j\pi \left[\sum_{m=-\infty}^{n} 2h_{(m)}\gamma_{m,\,1} \right] \right\} = b^{(1)}_{0,\,n-1} e^{j2\pi h_{(n)}\gamma_{n,\,1}} \tag{14}$$

$$b^{(0)}_{1,\,n} = \exp\left\{ j\pi \left[\sum_{m=-\infty}^{n} h_{(m)}\gamma_{m,\,0} - h_{(n-1)}\gamma_{n-1,\,0} \right] \right\} = b^{(0)}_{0,\,n-2} e^{j\pi h_{(n)}\gamma_{n,\,0}}. \tag{15}$$

This shows that $a_{7,\,n}$ is a function of the 3-tuple $\sigma_n = (\theta_{n-2}, \alpha_{n-1}, \alpha_n)$. Additional analysis shows that all of entries in Table 1 where $D_k = 2$ are a function of the same 3-tuple. Based on the 4 different values of D_k, the 48 pseudo-symbols and pulses can be grouped into the sets

$$K_j = \{k : D_k = 4 - j\}, \qquad 0 \le j \le 3. \tag{16}$$

These sets will be important in deriving reduced complexity receivers in the following sections.

Table 2: Laurent pulses for binary case, $L = 3$, $N_h = 2$

k	$c_{k,\,0}$
0	$[u_{0,\,0}u_{1,\,1}u_{2,\,0};\ u_{1,\,0}u_{2,\,1}u_{3,\,1};\ u_{2,\,0}u_{3,\,0}u_{4,\,1};\ u_{3,\,1}u_{4,\,0}u_{5,\,1}]$
1	$[u_{0,\,0}u_{4,\,1}u_{2,\,0};\ u_{1,\,0}u_{5,\,1}u_{3,\,1}]$
2	$[u_{0,\,0}u_{1,\,1}u_{5,\,0}]$
3	$[u_{0,\,0}u_{4,\,1}u_{5,\,0}]$

k	$c_{k,\,1}$
0	$[u_{0,\,1}u_{1,\,0}u_{2,\,1};\ u_{1,\,1}u_{2,\,0}u_{3,\,0};\ u_{2,\,1}u_{3,\,1}u_{4,\,0};\ u_{3,\,0}u_{4,\,1}u_{5,\,0}]$
1	$[u_{0,\,1}u_{4,\,0}u_{2,\,1};\ u_{1,\,1}u_{5,\,0}u_{3,\,0}]$
2	$[u_{0,\,1}u_{1,\,0}u_{5,\,1}]$
3	$[u_{0,\,1}u_{4,\,0}u_{5,\,1}]$

MAXIMUM LIKELIHOOD SEQUENCE ESTIMATING RECEIVER

The MLSE receiver for the equivalent PAM representation was derived by Kaleh [6], and requires only trivial extension to accommodate the multi-h case. The receiver has pM^{L-1} states, with M branches at each state. The state transitions and trellis diagram are identical to the optimal receiver presented in [2]. Here, the i-th branch in the trellis has a set of $N = 48$ pseudo-symbols $a^i_{k,(n)}$ associated with it. The branch metric for the i-th branch in the trellis is

$$\lambda_i(n) \equiv \text{Re} \sum_{k=0}^{N-1} z_{k,(n)} \bar{a}^i_{k,(n)} \tag{17}$$

$$z_{k,(n)} = \int_{nT}^{(n+D_k)T} r(t) g_{k,(n)}(t - nT)\, dt \tag{18}$$

$$r(t) = s(t, \boldsymbol{\alpha}) + n(t) \tag{19}$$

where $z_{k,(n)}$ is the output of the k-th matched filter at the n-th symbol interval, and $n(t)$ is additive white Gaussian noise (AWGN). Practically speaking, the limits of integration in Equation (18) require a delay of L symbol intervals, since $\max\{D_k\} = L + 1$.

The structure of this MLSE receiver is shown in Figure 1. The received signal $r(t)$ is fed into the bank of matched filters. The sampled filter outputs are the inputs to the Viterbi algorithm, which computes branch metrics, determines the surviving path at each merging node, and outputs a decision. Figure 2 shows an expanded view of the k-th filter in the bank. Each filter actually consists of a set of N_h filters whose sampled outputs are cyclically selected using a commutator and then delayed by the amount needed to have an overall filter delay of L symbol times.

Table 3: 4-ary pseudo-symbols, pulses, and pulse lengths for the ARTM Tier II case

k	$g_{k,(n)}(t)$	$a_{k,n}$	D_k
0	$c^{(0)}_{0,(n)}(t)c^{(1)}_{0,(n)}(t)$	$b^{(0)}_{0,n}b^{(1)}_{0,n}$	4
1	$c^{(0)}_{0,(n-1)}(t+T)c^{(1)}_{0,(n)}(t)$	$b^{(0)}_{0,n-1}b^{(1)}_{0,n}$	3
2	$c^{(0)}_{0,(n)}(t)c^{(1)}_{0,(n-1)}(t+T)$	$b^{(0)}_{0,n}b^{(1)}_{0,n-1}$	3
3	$c^{(0)}_{0,(n-2)}(t+2T)c^{(1)}_{0,(n)}(t)$	$b^{(0)}_{0,n-2}b^{(1)}_{0,n}$	2
4	$c^{(0)}_{0,(n)}(t)c^{(1)}_{0,(n-2)}(t+2T)$	$b^{(0)}_{0,n}b^{(1)}_{0,n-2}$	2
5	$c^{(0)}_{0,(n-3)}(t+3T)c^{(1)}_{0,(n)}(t)$	$b^{(0)}_{0,n-3}b^{(1)}_{0,n}$	1
6	$c^{(0)}_{0,(n)}(t)c^{(1)}_{0,(n-3)}(t+3T)$	$b^{(0)}_{0,n}b^{(1)}_{0,n-3}$	1
7	$c^{(0)}_{1,(n)}(t)c^{(1)}_{0,(n)}(t)$	$b^{(0)}_{1,n}b^{(1)}_{0,n}$	2
8	$c^{(0)}_{1,(n-1)}(t+T)c^{(1)}_{0,(n)}(t)$	$b^{(0)}_{1,n-1}b^{(1)}_{0,n}$	1
9	$c^{(0)}_{1,(n)}(t)c^{(1)}_{0,(n-1)}(t+T)$	$b^{(0)}_{1,n}b^{(1)}_{0,n-1}$	2
10	$c^{(0)}_{1,(n)}(t)c^{(1)}_{0,(n-2)}(t+2T)$	$b^{(0)}_{1,n}b^{(1)}_{0,n-2}$	2
11	$c^{(0)}_{1,(n)}(t)c^{(1)}_{0,(n-3)}(t+3T)$	$b^{(0)}_{1,n}b^{(1)}_{0,n-3}$	1
12	$c^{(0)}_{2,(n)}(t)c^{(1)}_{0,(n)}(t)$	$b^{(0)}_{2,n}b^{(1)}_{0,n}$	1
13	$c^{(0)}_{2,(n)}(t)c^{(1)}_{0,(n-1)}(t+T)$	$b^{(0)}_{2,n}b^{(1)}_{0,n-1}$	1
14	$c^{(0)}_{2,(n)}(t)c^{(1)}_{0,(n-2)}(t+2T)$	$b^{(0)}_{2,n}b^{(1)}_{0,n-2}$	1
15	$c^{(0)}_{2,(n)}(t)c^{(1)}_{0,(n-3)}(t+3T)$	$b^{(0)}_{2,n}b^{(1)}_{0,n-3}$	1
16	$c^{(0)}_{3,(n)}(t)c^{(1)}_{0,(n)}(t)$	$b^{(0)}_{3,n}b^{(1)}_{0,n}$	1
17	$c^{(0)}_{3,(n)}(t)c^{(1)}_{0,(n-1)}(t+T)$	$b^{(0)}_{3,n}b^{(1)}_{0,n-1}$	1
18	$c^{(0)}_{3,(n)}(t)c^{(1)}_{0,(n-2)}(t+2T)$	$b^{(0)}_{3,n}b^{(1)}_{0,n-2}$	1
19	$c^{(0)}_{3,(n)}(t)c^{(1)}_{0,(n-3)}(t+3T)$	$b^{(0)}_{3,n}b^{(1)}_{0,n-3}$	1
20	$c^{(0)}_{0,(n)}(t)c^{(1)}_{1,(n)}(t)$	$b^{(0)}_{0,n}b^{(1)}_{1,n}$	2
21	$c^{(0)}_{0,(n-1)}(t+T)c^{(1)}_{1,(n)}(t)$	$b^{(0)}_{0,n-1}b^{(1)}_{1,n}$	2
22	$c^{(0)}_{0,(n)}(t)c^{(1)}_{1,(n-1)}(t+T)$	$b^{(0)}_{0,n}b^{(1)}_{1,n-1}$	1
23	$c^{(0)}_{0,(n-2)}(t+2T)c^{(1)}_{1,(n)}(t)$	$b^{(0)}_{0,n-2}b^{(1)}_{1,n}$	2
24	$c^{(0)}_{0,(n-3)}(t+3T)c^{(1)}_{1,(n)}(t)$	$b^{(0)}_{0,n-3}b^{(1)}_{1,n}$	1
25	$c^{(0)}_{1,(n)}(t)c^{(1)}_{1,(n)}(t)$	$b^{(0)}_{1,n}b^{(1)}_{1,n}$	2
26	$c^{(0)}_{1,(n-1)}(t+T)c^{(1)}_{1,(n)}(t)$	$b^{(0)}_{1,n-1}b^{(1)}_{1,n}$	1
27	$c^{(0)}_{1,(n)}(t)c^{(1)}_{1,(n-1)}(t+T)$	$b^{(0)}_{1,n}b^{(1)}_{1,n-1}$	1
28	$c^{(0)}_{2,(n)}(t)c^{(1)}_{1,(n)}(t)$	$b^{(0)}_{2,n}b^{(1)}_{1,n}$	1
29	$c^{(0)}_{2,(n)}(t)c^{(1)}_{1,(n-1)}(t+T)$	$b^{(0)}_{2,n}b^{(1)}_{1,n-1}$	1
30	$c^{(0)}_{3,(n)}(t)c^{(1)}_{1,(n)}(t)$	$b^{(0)}_{3,n}b^{(1)}_{1,n}$	1
31	$c^{(0)}_{3,(n)}(t)c^{(1)}_{1,(n-1)}(t+T)$	$b^{(0)}_{3,n}b^{(1)}_{1,n-1}$	1
32	$c^{(0)}_{0,(n)}(t)c^{(1)}_{2,(n)}(t)$	$b^{(0)}_{0,n}b^{(1)}_{2,n}$	1
33	$c^{(0)}_{0,(n-1)}(t+T)c^{(1)}_{2,(n)}(t)$	$b^{(0)}_{0,n-1}b^{(1)}_{2,n}$	1
34	$c^{(0)}_{0,(n-2)}(t+2T)c^{(1)}_{2,(n)}(t)$	$b^{(0)}_{0,n-2}b^{(1)}_{2,n}$	1
35	$c^{(0)}_{0,(n-3)}(t+3T)c^{(1)}_{2,(n)}(t)$	$b^{(0)}_{0,n-3}b^{(1)}_{2,n}$	1
36	$c^{(0)}_{1,(n)}(t)c^{(1)}_{2,(n)}(t)$	$b^{(0)}_{1,n}b^{(1)}_{2,n}$	1
37	$c^{(0)}_{1,(n-1)}(t+T)c^{(1)}_{2,(n)}(t)$	$b^{(0)}_{1,n-1}b^{(1)}_{2,n}$	1
38	$c^{(0)}_{2,(n)}(t)c^{(1)}_{2,(n)}(t)$	$b^{(0)}_{2,n}b^{(1)}_{2,n}$	1
39	$c^{(0)}_{3,(n)}(t)c^{(1)}_{2,(n)}(t)$	$b^{(0)}_{3,n}b^{(1)}_{2,n}$	1
40	$c^{(0)}_{0,(n)}(t)c^{(1)}_{3,(n)}(t)$	$b^{(0)}_{0,n}b^{(1)}_{3,n}$	1
41	$c^{(0)}_{0,(n-1)}(t+T)c^{(1)}_{3,(n)}(t)$	$b^{(0)}_{0,n-1}b^{(1)}_{3,n}$	1
42	$c^{(0)}_{0,(n-2)}(t+2T)c^{(1)}_{3,(n)}(t)$	$b^{(0)}_{0,n-2}b^{(1)}_{3,n}$	1
43	$c^{(0)}_{0,(n-3)}(t+3T)c^{(1)}_{3,(n)}(t)$	$b^{(0)}_{0,n-3}b^{(1)}_{3,n}$	1
44	$c^{(0)}_{1,(n)}(t)c^{(1)}_{3,(n)}(t)$	$b^{(0)}_{1,n}b^{(1)}_{3,n}$	1
45	$c^{(0)}_{1,(n-1)}(t+T)c^{(1)}_{3,(n)}(t)$	$b^{(0)}_{1,n-1}b^{(1)}_{3,n}$	1
46	$c^{(0)}_{2,(n)}(t)c^{(1)}_{3,(n)}(t)$	$b^{(0)}_{2,n}b^{(1)}_{3,n}$	1
47	$c^{(0)}_{3,(n)}(t)c^{(1)}_{3,(n)}(t)$	$b^{(0)}_{3,n}b^{(1)}_{3,n}$	1

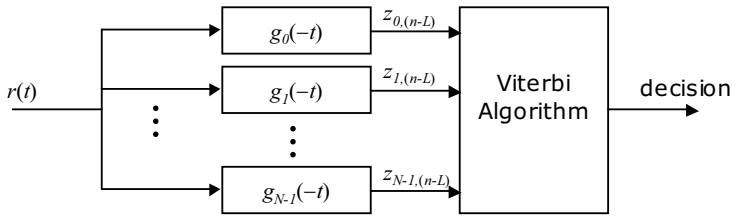

Figure 1: Linear MLSE receiver structure

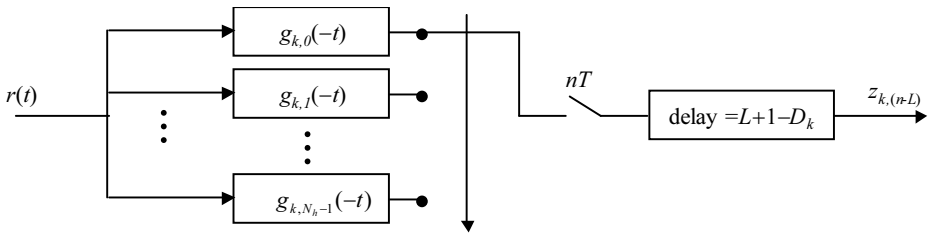

Figure 2: Expanded view of multi-h matched filter with delay

REDUCED COMPLEXITY RECEIVER

The linear decomposition of the CPM signal allows for some attractive complexity reductions. For example, in the ARTM Tier II case, the signal is fully described by 4-tuple $\sigma_n = (\theta_{n-3}, \alpha_{n-2}, \alpha_{n-1}, \alpha_n)$. This results in $32 * 4 * 4 = 512$ states, with 4 branches at each state. However, we can describe the pseudo-symbols in K_0 and K_1, as defined in Equation (16), with only two values: (θ_{n-1}, α_n). A signal composed of these three pseudo-symbols and their respective pulses has only 32 states. Numerical calculations show that these first three pulses contain 98.26% and 98.49% of the signal energy at even and odd symbol times respectively. If we include the pulses in K_2 we account for 99.999% of the signal energy and have a signal with 128 states. The reduced complexity receivers described in these examples have the branch metric

$$\lambda_i(n) \equiv \text{Re} \sum_{k \in K} z_{k,(n)} \bar{a}^i_{k,(n)} \tag{20}$$

where K is a subset of indices as described in the examples above.

Further complexity reduction can be made by reducing the number of matched filters. For example, the multi-h nature of the signal increases the number of filters required by a factor of N_h, as Figure 2 demonstrates. However, if the difference between the N_h filters for a given k is negligible, then one filter might be used to approximate the set of N_h filters. This is illustrated in Figure 3a. The fact that the pulses in this figure are difficult to distinguish from each other underscores the point. There are three "groups" of pulses, one each for $k = 0, 1, 2$. In each group, there is a pair of individual pulses: even symbol times (solid line) and odd symbol times (dashed). The group with the largest pulses is $k = 0$ (which is the set K_0), the smaller pulses are $k = 1, 2$ (which is the set K_1). While there is a slight difference between the even and odd pulses, the average of the two pulses can be used in the receiver with a performance loss of a few tenths of a dB, as shown in the following section. This averaging reduces the filter-commutator-delay structure in Figure 2 to a single filter $g_k(-t)$ followed by the delay element.

There are additional filter reductions that can be made on an ad hoc basis. In Figure 3a, all four pulses in K_1 are very similar, and can be averaged over K_1 in addition to averaging over h to give a single pulse $g_{K_1}(t)$. This can also be applied to the pulses in K_2. A close-up view of the 9 h-averaged pulses in K_2 is shown in Figure 3b. These 9 pulses can be represented by a single averaged pulse $g_{K_2}(t)$, and then scaled by d_k, where d_k minimizes the mean-squared error

$$d_k = \arg\min_d \int_0^{D_k T} \left(d \cdot g_{K_2}(t) - g_k(t) \right)^2 dt. \tag{21}$$

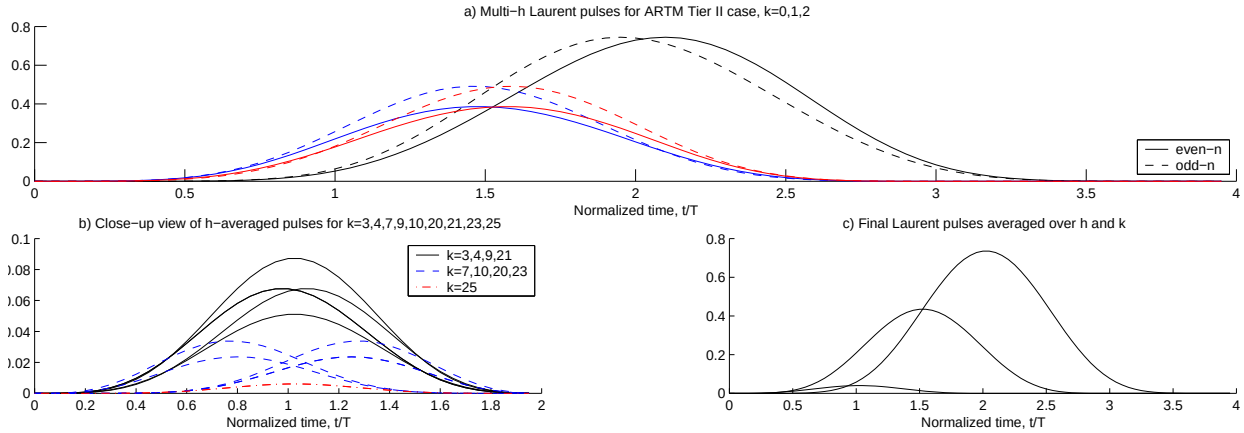

Figure 3: a) Pulses for $k = 0, 1, 2$. The solid lines are for even symbol times and the dashed lines are for odd symbol times. b) Close-up view of the 9 pulses in the set K_2. c) Final three pulses in order from largest to smallest, $g_{K_0}(t)$, $g_{K_1}(t)$, and $g_{K_2}(t)$.

This scale factor can be applied offline to the pseudo-symbols

$$a^i_{K_2,(n)} = \sum_{k \in K_2} d_k a^i_{k,(n)}. \tag{22}$$

The same technique can be applied to the two pulses in $g_{K_1}(t)$. This simplified receiver with only three filters has the branch metric

$$\lambda_i(n) \equiv \mathrm{Re}\left\{ \bar{a}^i_{K_0,(n)} z_{K_0,\,n} + \bar{a}^i_{K_1,(n)} z_{K_1,\,n} + \bar{a}^i_{K_2,(n)} z_{K_2,\,n} \right\} \tag{23}$$

where the modulo-N_h notation (n) has been dropped on $z_{K_j,\,n}$ due to the averaging over h. These final three pulses are shown in Figure 3c. It is important to point out that the pseudo-symbols $a^i_{K_j,(n)}$ on each branch still vary from even to odd symbol-times, as do the state transitions in the trellis. This implies that there will still be a multi-h performance gain in this receiver.

PERFORMANCE

The performance of these receivers was investigated using computer simulations. Four receivers were simulated. The first is the optimal MLSE receiver described by Equation (17). The second is the 32-state receiver using the pseudo-symbols and pulses in the set $K = \{0, 1, 2\}$ (K_0 and K_1). The pulses in this second receiver not averaged in any way. This is the receiver recommended by Mengali [4] for the $M = 4$ case. The third receiver uses the averaged pulses for K_0–K_2. The trellis for this receiver is a function of $\sigma_n = (\theta_{n-2}, \alpha_{n-1}, \alpha_n)$ and requires a 128-state trellis. An additional simplification is made by using the surviving symbol $\hat{\alpha}^i_{n-1}$ at each state, rather than accounting for α_{n-1} in the trellis. This reduces the trellis to 32 states. The fourth receiver is the single-h MLSE receiver for $h = 1/4$, $M = 4$, 3RC, which is spectrally similar to the ARTM Tier II waveform. It is included to provide a single-h/multi-h comparison.

Figure 4 shows the simulated bit error rate (BER) vs. E_b/N_0 for each of these four receivers. There are a number of significant observations to be made. As expected, the performance of the MLSE receiver

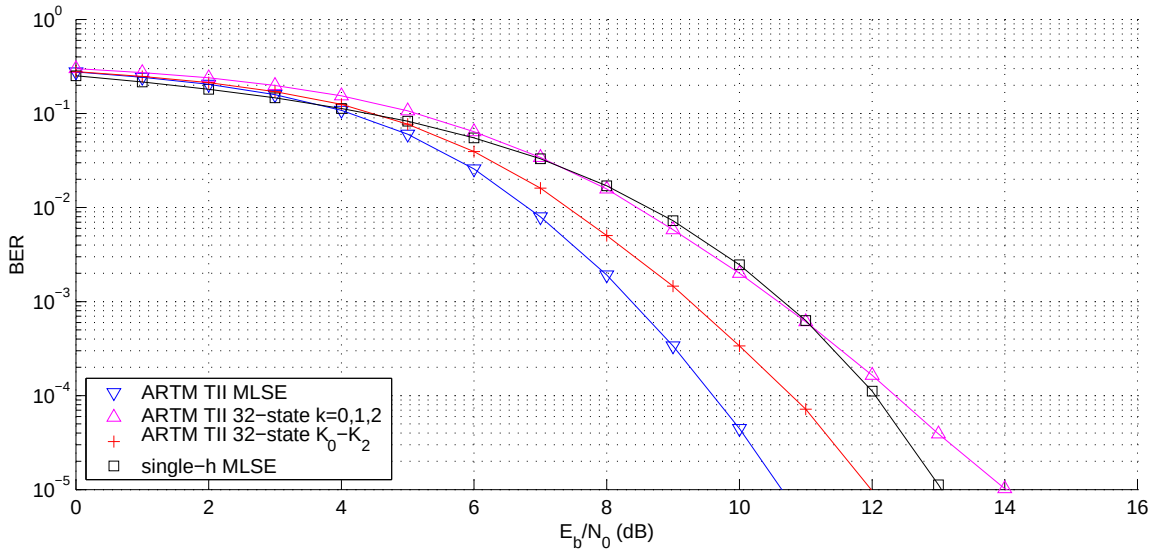

Figure 4: Performance of the four receivers simulated. The performance loss relative to the optimum receiver at BER $= 10^{-5}$ is 3.5 dB for the 32-state $k = 0, 1, 2$ receiver. The performance loss for the 32-state K_0–K_2 receiver at the same point is 1.5 dB. The figure also shows that a multi-h gain is achieved with the simplified PAM receiver against a MLSE receiver using a comparable single-h scheme.

presented in this paper exactly matches previously reported results [5] for the existing MLSE receiver in [2]. The second receiver (32-state $k = 0, 1, 2$) has a performance loss of 3.5 dB relative to the optimum at BER $= 10^{-5}$. The loss narrows at higher bit error rates. The third receiver (32-state K_0–K_2) has a performance loss of only 1.5 dB relative to optimum at the BER $= 10^{-5}$ operating point. The 2 dB gain of the third receiver over the second is surprising given the similar complexity of the receivers (three filters, 32 states). The important difference between the two receivers is that the third receiver accounts for an additional symbol in memory ($\hat{\alpha}^i_{n-1}$). This accounting produces appreciable results despite using previous decisions (instead of a 128-state trellis) and a highly averaged pulse with a very small amplitude ($g_{K_2}(t)$, shown in Figure 3c). The 1.5 dB loss of the third receiver was further explored by taking an additional simulation point for each of the approximations at the BER $= 10^{-5}$ operating point. The averaging all 48 pulses over even and odd symbol-times has a loss of 0.2 dB. The reduction to a 128-state trellis with K_0–K_2 has an additional loss of 0.1 dB. The 32-state trellis approximation using $\hat{\alpha}^i_{n-1}$ incurs a further loss of 0.9 dB. Finally, the pulse averaging over K_1 and K_2 adds a loss of 0.3 dB, for a total loss of 1.5 dB.

All of these simplifications allow for a multi-h gain; meaning a simplified multi-h receiver should out perform a similarly simplified single-h receiver. However, comparison of the third receiver with the fourth (single-h) shows that a much-simplified multi-h receiver can outperform the *optimal* receiver for a similar single-h scheme. This single-h scheme requires a 128-state trellis with 64 matched filters.

DISCUSSION AND CONCLUSIONS

The linear PAM multi-h CPM receivers presented in this paper are a viable alternative to the existing MLSE receiver for several reasons. The first is that the linear decomposition is very flexible and allows many different possibilities for significant complexity reduction. These approximations include averaging the signal pulses over h, averaging the pulses over common pulse-duration, and reducing the number of trellis states. In particular, it was found that even highly averaged pulses with small amplitudes could have a significant impact on receiver performance. The loss incurred by these approximations is small, ranging from fractions of a dB to 3.5 dB for an extreme case. One attractive receiver required only three matched filters and a 32-state trellis and incurred a loss of only 1.5 dB. Another advantage is that the approximations preserve the multi-h gain in the signal. This gain is often lost when using reduced-complexity receivers [2, 5]. A further advantage is that it results in a linear receiver, and linear techniques can be applied to other receiver design problems such as synchronization.

Future work in this area will include a general presentation of the equivalent PAM representation for the M-ary multi-h case. Further work might also derive an analytical expression for receiver performance. Such an expression might also lead to methods of optimizing the various approximations presented here. There is also work to be done regarding receiver synchronization.

REFERENCES

[1] M. Geoghegan. "Description and performance results for the advanced range telemetry (ARTM) Tier II waveform". In *Proceedings of the International Telemetering Conference*, San Diego, CA, October 2000.

[2] J. B. Anderson, T. Aulin, C-E. Sundberg. *Digital Phase Modulation*. Plenum Press, New York, 1986.

[3] P. A. Laurent. "Exact and approximate construction of digital phase modulations by superposition of amplitude modulated pulses (AMP)". *IEEE Transactions on Communications*, 34:150–160, February 1986.

[4] U. Mengali and M. Morelli. "Decomposition of M-ary CPM signals into PAM waveforms". *IEEE Transactions on Information Theory*, 41:1265–1275, September 1995.

[5] E. Perrins and M. Rice. "Comparison of receivers for multi-h CPM". In *Proceedings of the International Telemetering Conference*, San Diego, CA, October 2002.

[6] G. K. Kaleh. "Simple coherent receivers for partial response continuous phase modulation". *IEEE Journal on Selected Areas in Communications*, 7:1427–1436, December 1989.